Radiative and Auger rates of high doubly excited states of multiply charged heliumlike ions

BingCong Gou,* Z. Chen, and C. D. Lin
Department of Physics, Kansas State University, Manhattan, Kansas 66506
(Received 5 October 1990)

The radiative and Auger rates of doubly excited states of positive ions where the principal quantum numbers of both electrons are large (≥ 6) are studied using a restricted-configuration-interaction method. The partial radiative and Auger rates to final states are calculated for doubly excited states of Ar^{16+}. It is shown that the propensity rule for both the radiative and Auger decay is $\Delta v = v_f - v_i = 0$, where v is the bending vibrational quantum number of the doubly excited state. Systematics of the radiative and Auger rates along different sequences of doubly excited states are also investigated.

I. INTRODUCTION

Doubly excited states of atoms and ions have been studied over the past few decades both theoretically and experimentally. In most of these investigations, doubly excited states are populated by electron, photon, or ion impact from the ground states of target atoms. The states populated in these collisions are low-lying doubly excited states where the principal quantum number of at least one of the electrons is small. In recent years, doubly excited states where the principal quantum numbers of both electrons are large have been studied experimentally either by two-step laser excitations[1,2] or through double-capture processes in the collision of multiply charged ions with multielectron targets.

While some gross features of these doubly excited states can be estimated from the experimental data under a number of assumptions, a deeper understanding of the subject requires the knowledge of properties such as the energy levels and the radiative and Auger decay rates of these states. Such information cannot be derived from the experimental data since the energy resolution in general is not enough to separate individual states.

From the theoretical viewpoint, information on doubly excited states where the principal quantum numbers are large is complicated by two factors: (1) Electron correlation plays a major role in doubly excited states and configuration interaction must be considered for the calculation of energy and decay rates for each state; (2) the number of states within a narrow energy range and the possible number of decay channels for each state are very large. To compile such information for a certain subset of doubly excited states useful for experimentalists is a formidable job.

In this article we study the decay properties of doubly excited states where the principal quantum numbers of both electrons are large. Our goal is to find out if there are some simple systematics which are of general significance. In particular, we wish to identify simple approximate selection rules, or propensity rules, for the radiative and Auger decay rates. These rules isolate the few major decay channels for each group of doubly excited states.

The propensity rules for autoionization processes have been discussed qualitatively in previous studies using hyperspherical potential curves,[3,4] or in terms of molecular-orbital (MO)-type potential curves.[5] The systematics along the rotor series has been discussed by Chen and Lin.[6] These discussions are limited to doubly excited states where the principal quantum numbers are relatively small (≤ 6). The propensity rule has also been studied by Matsuzawa and co-workers[7,8] for the generalized oscillator strengths for transitions between doubly excited states of helium atoms using wave functions obtained by the hyperspherical approach. Note that in the optical limit, the generalized oscillator strength is proportional to the dipole oscillator strength and thus the same propensity rule is expected. In our calculation we sample a much larger number of transitions using the simpler configuration-interaction CI wave functions. For simplicity we concentrate on doubly excited states of Ar^{16+} where the principal quantum numbers of both electrons are in the range of 6–10. The selection of Ar^{16+} makes the calculation of the decay properties easier, but the derived propensity rules are expected to work for other systems.

Knowledge of the radiative and Auger rates of doubly excited states is important in understanding the stabilization of doubly excited states formed in collisions between multiply charged ions with atoms, molecules, and surfaces. The branching ratio for the radiative decay with respect to the Auger decay determines whether doubly excited states will be observed as transfer ionization or true double capture.[9] An estimate of the lifetimes of these states is also needed for the understanding of the formation of "hollow atoms" in ion-surface collisions.[10] An existing estimate of the lifetimes of such doubly excited states has been based on the simple hydrogenic model[11] or single configuration model[12] where the important configuration interaction has been completely neglected.

In this paper we us the simple configuration-interaction method to calculate the energies and the radiative and Auger decay rates of doubly excited states where the principal quantum numbers of both electrons are large. To sort out the systematics, we first review the designation of doubly excited states in Sec. II, while the

restricted configuration-interaction method and the calculation of Auger and radiative rates are discussed in Sec. III. The results are presented in a number of subsections in Sec. IV, and the final conclusion is given in Sec. V.

II. DESIGNATION AND SYSTEMATICS OF DOUBLY EXCITED STATES

According to the independent electron model, each doubly excited state can be represented by the notation $Nlnl'$, in addition to the exact quantum numbers L, S, and π (relativistic effects are neglected completely in this work). The N and n are the principal quantum numbers of the inner and the outer electrons, respectively. For simplicity, the subset of states with fixed N, n, L, S, and π, will be called to form a *manifold* of states. For the high-Z ions considered here, the splitting of levels within a manifold is small compared to that of states from different manifolds. Since configuration interaction is large, the notation $Nlnl'$ is inadequate, and l and l' should be replaced by quantum numbers K, T, and A such that each state is designated[13-15] by ${}_n(K,T)_N^A\ {}^{2S+1}L^\pi$. The approximate quantum numbers K, T, and A have simple geometric meanings. In particular, K has to do with the nodal structure of the wave function in angle θ_{12} between the two electrons with respect to the nucleus. It is also related to the bending vibrational quantum number $v=N-K-1$. T is the projection of L along the interelectronic axis and A is $+1$ (-1) for symmetric (antisymmetric) stretches. If the doubly excited state does not have symmetric or antisymmetric stretches, then its vibrational motion is similar to the local modes in molecules and $A=0$ is assigned for such states. The enumeration of the quantum numbers K and T for states within a given manifold has been described previously.[13-15]

According to the ${}_n(K,T)_N^A\ {}^{2S+1}L^\pi$ designation, there are a number of sequences that can be identified depending on which set of quantum numbers are being fixed.

(a) Simple Rydberg series: This is the series of states ${}_n(K,T)_N^A\ {}^{2S+1}L^\pi$ with all the quantum numbers fixed except for n. The correlation pattern for all the states within the Rydberg series remains nearly independent of n. If the wave function is expressed as $F(R)\Phi(R;\Omega)$, then $\Phi(R;\Omega)$ remains roughly the same for all the states while the number of nodes in $F(R)$ increases by one for each increasing value of n.[16] This is similar to the simple Rydberg series for singly excited states except that each state is not represented by a single configuraiton.

(b) Rotor series: This is the series of states ${}_n(K,T)_N^A\ {}^{2S+1}L^\pi$ for fixed ${}_n(K,T)_N^A$ with varying L, S, and π. Each successive member of the rotor series has one more unit of angular momentum than the previous member and two neighboring states have opposite π (even or odd) and S (singlet or triplet). The rotor series terminates at a certain $L_{\max}$.[13,14] The correlation pattern for members of the rotor series remains nearly constant, and higher L corresponds to higher rotational excitations.

(c) Vibrational series: This pertains to the states in the manifold for fixed n, N, L, S, and π. Using $v=N-K-1$, the states within the manifold have different vibrational quantum numbers v and the wave functions have different nodal structures in θ_{12}.

(d) Double-Rydberg series: This pertains to intrashell states ${}_N(K,T)_N^A\ {}^{2S+1}L^\pi$ which have the fixed vibrational quantum number $v=N-K-1$, in addition to fixed T, L, S, and π. The principal quantum number N of both electrons changes by one unit along the series but with the values of v fixed. States within the double-Rydberg series have a fixed number of nodes in θ_{12}.

III. THE CALCULATION OF ENERGIES AND RADIATIVE AND AUGER RATES OF DOUBLY EXCITED STATES

A. Restricted configuration-interaction approach

Doubly excited states can be calculated using different theoretical approaches. For the present purpose, it is desirable that each wave function and the radiative and Auger rates be easily calculated. To this end, we adopt the conventional configuration-interaction (CI) approach but each state is labelled using the ${}_n(K,T)_N^A\ {}^{2S+1}L^\pi$ designation. The CI approach is convenient for obtaining many wave functions in a single calculation. On the other hand, the CI approach is known to converge slowly for neutral atoms and for low-Z ions if the hydrogenic wave functions are used as basis functions.[17] We avoid this limitation by performing calculations for the heliumlike Ar. For such a system, configuration interaction between states belonging to different shells is small and can be neglected in general. In other words, for each L, S, and π, only the intrashell coupling between the $Nlnl'$ states with fixed N and n is to be included. We mention that for neutral and low-Z ions a better starting point is to use the multiconfiguration Hartree-Fock approach for each orbital.[18]

Our method of calculation is best illustrated by an example. To obtain the six wave functions within the $6l6l$ ${}^1S^e$ manifold, two-electron product wave functions $|6l6l\ {}^1S^e>$ are constructed where each $6l$ is a hydrogenic orbital with effective charge Z^*. The six basis functions are used to diagonalize the two-electron Hamiltonian. The effective charge Z^* is obtained variationally to give the minimum energy for the lowest state. It is clear that in this approach the CI includes only the angular correlation, while the radial correlation is partially accounted for by the effective charge Z^*. Limiting the selection to $6l6l$ configurations only avoids the variational collapse when the effective charge is varied. To check the accuracy of this appraoch, we also include in the CI calculations basis functions for states such as $mlnl$ ${}^1S^e$ $(n,m>6)$, where each orbital is a hydrogenic wave function with Z^*. For Ar^{16+}, the mixing of $6l6l$ states with these latter configurations is small, even for the higher energy states within the $6l6l$ ${}^1S^e$ manifold.

This approach is similar to the earlier extensive CI calculations carried by Lipsky, Anania, and Conneely[17] for the low-lying doubly excited states ($Nlnl'$ states for $N\leq 3$) of He-like ions. We used this method to calculate the energy levels of the $3l3l'$ and $4l4l'$ doubly excited

states of C^{4+} and O^{6+}, and the results[19] were found in good agreement with those calculated by Ho[20] and by Bachau[21] as well as with experiments.[22] The method has also been used to calculate the energy levels of $3l3l'$ states of Be-like ions[23] where the results are in good agreement with experiments and with other calculations. In this article we extend this method to doubly excited states where the principal quantum numbers of both electrons are large. We concentrated on the $6l6l'$ doubly excited states. There are already quite a large number of states within this manifold, and the possible number of radiative and Auger decay channels for each state is quite large. The propensity rules derived from this calculation can be applied to other $NlNl'$ intrashell states of higher N, and for other two-electron ions. We mention that there are no systematic investigations of such high-lying doubly excited states both theoretically and experimentally except for the photoabsorption studies in H^- (Refs. 24 and 25) and in He.[26]

Our approach gives a slightly different effective charge for states within different manifolds. For intershell states, we actually constuct two-electron states where the inner electron "sees" a charge $Z=18$, and the outer electron "sees" a charge $Z=17$ (symmetrization of the wave function is included). The wave functions thus calculated are not orthogonal, but such nonorthogonality is accounted for in the calculation of radiative and Auger matrix elements.

B. Doubly-excited-state basis (DESB) functions

Approximate doubly-excited-state wave functions for intrashell states of two-electron systems have been obtained from the group-theoretical consideration by Herrick and Sinanoglu.[15] They are called the doubly-excited-state basis (DESB) functions where each state is designated by the K and T quantum numbers. The DESB functions can be considered as approximate CI functions where the CI coefficients are given analytically in terms of 9-j symbols. In essence, the DESB functions include most of the intrashell angular correlation, which is the dominant correlation for doubly excited states of high-Z ions. For semiquantitative analysis we can use DESB functions to calculate radiative and Auger rates.

C. Calculation of radiative and Auger rates

With the initial- and final-state wave functions calculated as described above, the radiative rates averaged over the initial magnetic substates Ψ_i and summed over the final magnetic states Ψ_f are calculated (in a.u.) by

$$W_R=2\alpha^3\omega^2 f \ , \tag{1}$$

where f is the oscillator strength and ω is the energy separation between the initial and final states. The Auger width, according to the golden rule, is calculated (in Ry) by

$$\Gamma_A=4\pi|\langle\Psi_i|1/r_{12}|\Psi_f\rangle|^2 \ , \tag{2}$$

which is converted to the Auger rate (in mRy) by

$$W_A(10^{12}/\mathrm{s})=20.6\Gamma_A \ . \tag{3}$$

IV. RESULTS AND DISCUSSION

A. Final states populated by radiative and Auger decays from the initial $_6(5,0)_6^+\ ^1S^e$ state

For doubly excited states where both electrons are highly excited, there are many final states that can be reached by radiative or Auger processes. In this section, we examine the partial radiative and Auger rates to each of the final states.

1. Dependence on the principal quantum numbers of final states

In terms of the CI representation the initial $_6(5,0)_6^+\ ^1S^e$ state is given primarily as a linear combination of configurations $6l^2$ ($l=0$–5). Since the radiative process is given by the one-body dipole operator, the final states populated are $_n(K,T)_N^A\ ^1P^o$, where $n=6$. In other words, the principal quantum number of one of the electrons remains the same, with the other electron making transitions to smaller $N<6$. There is no selection rule on the values of l and l' of the final states since, except for the $1snp$ state, the final states are doubly excited states, and configuration mixing for each state is large.

In Table I we list the Auger energy ϵ (for transitions to

TABLE I. Auger energies, partial Auger rates, partial radiative rates, and branching ratios of the decay of the $_6(5,0)_6^+\ ^1S^e$ state of Ar^{16+}. The integer N refers to the principal quantum number of the inner electron in the final state. Auger decay to the $5l\epsilon l$ states is not energetically allowed.

N	Auger energy (Ry)	Auger rate (10^{12} s^{-1})	Branching ratio ($\times 100$)	Radiative rate (10^{12} s^{-1})	Branching ratio ($\times 100$)
1	306.397	0.25	0.7	4.11	11.0
2	63.397	2.79	7.5	0.84	2.2
3	18.397	7.94	21.2	0.29	0.8
4	2.647	20.96	56.0	0.14	0.4
5				0.07	0.2
Total		31.94	85.4	5.45	14.6

$Nl\epsilon l$ states), the total Auger and radiative rates to each of the principal quantum number $N(<6)$. The branching ratio for each transition is also shown. We note that the Auger decay tends to populate the highest energetically allowed N, while the radiative decay tends to populate the lowest N. The Auger rate decreases rapidly with decreasing N and the radiative rate decreases rapidly with increasing N. The branching ratio for the total Auger processes is 85% and for the radiative processes is 15%.

2. *The propensity rule for radiative decays*

The radiative decay rate, as shown by Eq. (2), is proportional to $\omega^3 D^2$, where ω is the energy difference and D is the dipole matrix element, between the initial and final states. The radiative rate is dominated by $N=1$ since ω is largest for such a transition. Among the possible final $Nl6l'$ states for a fixed N, the ω for different states are comparable and thus the radiative rates reflect the magnitude of the dipole matrix elements, or the degrees of overlap between the wave functions of initial and final states, weighted by the dipole operator. In Table II, we show the oscillator strengths of the dominant final states populated by the radiative process to each N. Among the $2N-1$ final states (each is labeled by the quantum numbers K, T, A, and v_f) that are allowed for each N ($n=6$), only one state ($v_f=0$) is populated predominantly. We note that these states have identical vibrational quantum number as the initial state ($v_i=0$). Thus the propensity rule for the radiative transition is $\Delta v=0$.

To understand this propensity rule, we compare in Fig. 1 and Fig. 2, respectively, the hyperradial wave functions $F(R)$, and the charge density and the contour plots of the initial and the five final states belonging to $N=3$. To this end, each CI wave function is rewritten as $F(R)\Phi(R;\Omega)$, where $R=(r_1^2+r_2^2)^{1/2}$ (r_i is the radial distance of the electron i from the nucleus) is the hyperradius and Ω the five angles. Plotted in Fig. 1 are the functions $|R^{1/2}F(R)|$ and in Fig. 2 are the functions $|\Phi(R;\Omega)|^2$ at $R=3$ on the (α,θ_{12}) plane [$\alpha=\arctan(r_2/r_1)$] after being averaged over the rotation of the whole atom. Among the five final states, the radial functions $F(R)$ are quite similar, thus the large difference in the oscillator strength is attributed to the degree of overlap in the angular functions $\Phi(R;\Omega)$ between the initial and final states. Since the initial state is concentrated in the large-θ_{12} region, the final states populated are those which have large distributions in the large-θ_{12} region (see Fig. 2).

TABLE II. Oscillator strengths for the radiative decay of the ${}_6(5,0)_6^+\ {}^1S^e$ state of Ar^{16+}. The final doubly excited states are approximated by the DESB functions. The bending vibrational quantum number of the initial state is $v_i=0$. Note that the dominant final states populated have $v_f=0$. Final states with large v_f are not populated. The states for which $10^2 f<0.01$ are omitted.

n	N	K	T	A	v_f	$10^2 f$
6	1	0	0	0	0	1.45
6	2	1	0	−1	0	6.05
		0	1	+1	1	0.44
		−1	0	0	2	0.05
6	3	2	0	−1	0	16.11
		1	1	+1	1	1.12
		0	0	−1	2	0.09
6	4	3	0	−1	0	44.61
		2	1	+1	1	2.27
		1	0	−1	2	0.08
6	5	4	0	−1	0	181.90
		3	1	+1	1	5.19
		2	0	−1	2	0.05

3. *The propensity rule for Auger decays*

The ${}_6(5,0)_6^+\ {}^1S^e$ initial state can also decay by Auger transitions, with the final states represented by $Nl\epsilon l\ {}^1S^e$. In Table I we show the dominant N populated is $N=4$, since $N=5$ states are not allowed energetically. The Auger rate to each final $Nl\epsilon l\ {}^1S^e$ state for different l is quite comparable. For example, for $N=4$, the relative rates for $l=0,1,2,3$ are 1.0, 6.4, 5.3, and 0.6, respectively.

The propensity rule for the Auger process can be obtained if the final states are expressed in terms of eigen-

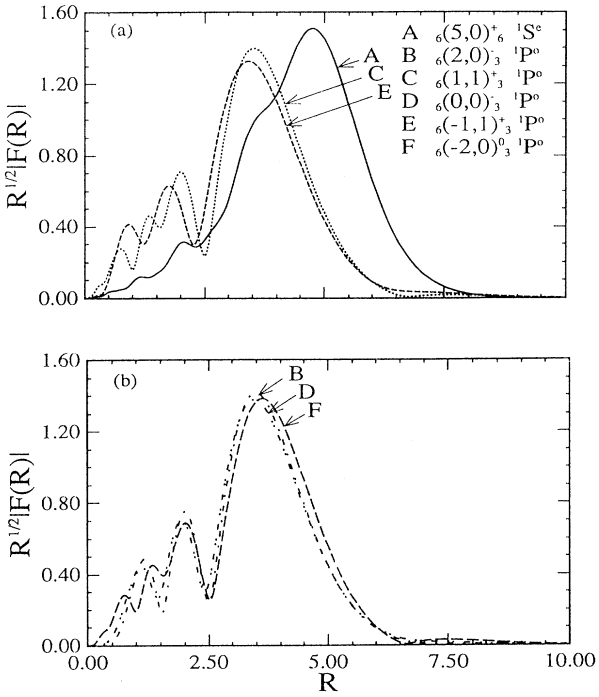

FIG. 1. Absolute values of the weighted hyperradial wave functions of the (A) initial state ${}_6(5,0)_6^+\ {}^1S^e$ and of the final states: (B) ${}_6(2,0)_3\ {}^1P^o$, (C) ${}_6(1,1)_3^+\ {}^1P^o$, (D) ${}_6(0,0)_3^-\ {}^1P^o$, (E) ${}_6(-1,1)_3^+\ {}^1P^o$, and (F) ${}_6(-2,0)_3^0\ {}^1P^o$.

channels in the context of the multichannel quantum defect theory. In the present case these eigenchannels can be easily obtained. Such eigenstates in the continuum are the continuation of the bound doubly excited states designated by ${}_n(K,0)_N^+ \, {}^1S^e$, as $n \to \infty$. In the present calculation, we assume that these eigenstates can be approximated by the DESB states where the mixing coefficients are evaluated for $N=6$ and $n=20$. Since there is little n dependence of the DESB functions for each channel ${}_n(K,0)_N^+ \, {}^1S^e$, such a representation for the eigenstates ${}_\epsilon(K,0)_N^+ \, {}^1S^e$ in the continuum is quite useful. If the Auger rate is calculated with respect to each such an eigenchannel (labelled by a vibrational quantum number v_f), strong selectoin rules for the Auger rates can be found. The calculated Auger widths with respect to v_f are shown in the histogram in Fig. 3. The propensity rule of $\Delta v=0$ is quite apparent for higher N. Transitions involving a large change in Δv have negligible Auger widths. The large width for $v_f=v_i$ can be attributed to the isomorphism of the electron correlation pattern between initial and final states.

To summarize this section, we reiterate that Auger transitions tend to populate final $Nl\epsilon l$ states with largest N which are energetically possible, and the radiative process tends to decay to $1s6p \, {}^1P^o$ state which has the largest photon energy. For the doubly excited states or continuum states within a given N manifold, the propensity rule for radiative and Auger processes is $\Delta v=0$.

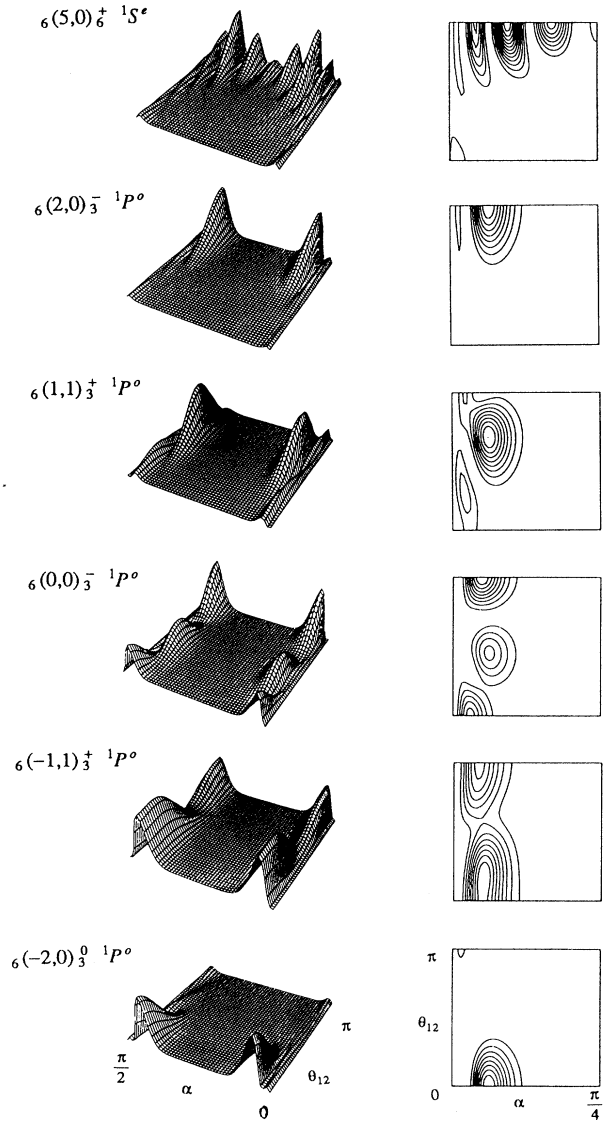

FIG. 2. Surface and contour plots of the electron density on the (α,θ_{12}) plane at $R=3$ for the states indicated.

B. Radiative and Auger decays of the states within the $6l6l \, {}^1S^e$ manifold

1. Total radiative and Auger rates

The partial Auger and radiative rates for the six states within the $6l6l \, {}^1S^e$ manifold are displayed in Table III. These states, which are classified with the $(K,0)^+$ quantum numbers, can be viewed as the sequence of vibrational states within the $6l6l$ manifold. The total Auger rate increases initially with decreasing values of K, reaching the maximum near $K=1$, and decreases for further negative values of K. The total radiative rates remain quite small along the sequence such that the Auger yield for the whole sequence is nearly unity except for the last member of the sequences which has an Auger yield of only 46%.

Comparing the partial Auger decays among the states listed in Table III, the dominant decay channel is still to

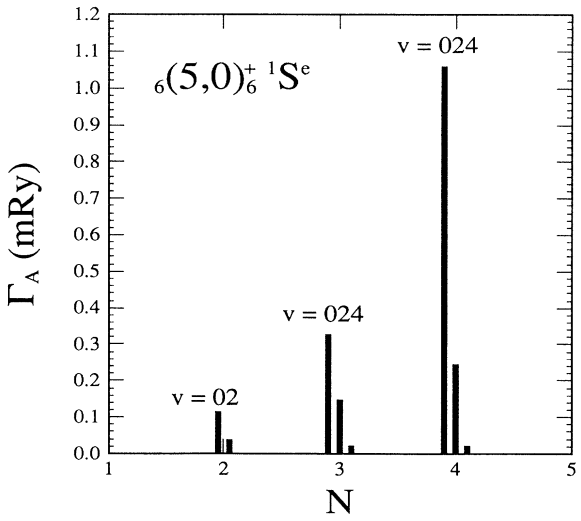

FIG. 3. The partial Auger widths for the ${}_6(5,0)_6^+ \, {}^1S^e$ state of Ar^{16+} on the principal quantum number N and the bending vibrational quantum number v of the final states. The initial state has $v=0$. The histogram shows that $v=0$ states are preferentially populated.

TABLE III. Dependence of partial Auger rates, radiative rates, and branching ratios of the ${}_6(K,0)_6^+ \ {}^1S^e$ states of Ar^{16+} on the principal quantum number N of the inner electron of the final states. Doubly excited states are calculated by CI. The binding energies are also given. The rates are given in units of $10^{12}\ s^{-1}$.

(K,T)	(5,0)		(3,0)		(1,0)		(−1,0)		(−3,0)		(−5,0)	
$-E$ (Ry)	17.603		17.510		17.383		17.207		16.948		16.459	
N	Γ_A	Γ_R	Γ_A	Γ_R	Γ_A	Γ_R	Γ_A	Γ_R	Γ_A	Γ_R	Γ_A	Γ_R
1	0.254	4.171	0.043	0.344	0.003	0.020	0.000	0.185	0.001	0.255	0.001	0.183
2	2.757	0.887	2.167	0.494	1.408	0.159	0.272	0.046	0.031	0.147	0.004	0.166
3	7.892	0.317	26.743	0.344	8.971	0.176	7.823	0.083	0.859	0.070	0.015	0.153
4	20.810	0.147	107.021	0.187	186.562	0.196	92.770	0.139	28.718	0.048	0.547	0.156
Total	31.715	5.524	135.976	1.371	196.946	0.553	100.865	0.455	29.610	0.521	0.568	0.660

the highest N values allowed. For the radiative decays, the partial rates do not maximize at the lowest values of N for the higher vibrational states within the manifold. This point is further discussed below.

2. *The propensity rule for radiative and Auger rates*

In order to elucidate the propensity rule of the radiative and Auger decay rates we first show in Fig. 4 the density plots of the six initial states in the $6l6l\ {}^1S^e$ manifold. The plots show that higher vibrational states indeed display more nodal structures along the θ_{12} axis and that the charge distribution moves progressively toward smaller θ_{12} with decreasing K (or increasing v).

The propensity rule for the radiative rates for the states within the $6l6l\ {}^1S^e$ manifold can be seen from Table IV. Both initial and final states are labelled by the K and T quantum numbers, but for the present purpose the vibrational quantum numbers v_i and v_f are more relevant. In Table IV, each $\Delta v=0$ transition is underlined with a solid line if it is the dominant transition. From the table it is clear that $\Delta v=0$ is indeed the dominant transition in most cases. Even if $\Delta v=0$ is not the dominant one (underlined with dashed lines), transitions that involve large Δv tend to have smaller oscillator strengths. If the initial state has a large value of v_i and all the final states have smaller values of v_f, then final states involving smaller Δv are predominantly populated. We further comment that since the $1s6p$ state has $v_f=0$, radiative transitions from $v_i \neq 0$ states to the $1s6p$ state are small. This explains why the total radiative decay rates for all the initial $v_i \neq 0$ states are smaller.

Similar approximate selection rules can be obtained for Auger decay rates, as shown in Table V for the Auger decay to the $N=4$ limit. Auger rates from the last two states ($v_i=8$ and 10, respectively) are smaller. Among the final states in the $N=4$ manifold, the largest v_f is 6 and thus the $\Delta v=0$ selection rule cannot be satisfied for $v_i=8$ and 10. For the $v_i=10$ state the smallest $\Delta v=4$. This accounts for its small Auger rate.

C. Systematics of total Auger and radiative rates along the rotor series

The partial, as well as the total, Auger and radiative rates for the second (${}^3P^0$) and the third (${}^1D^e$) member of

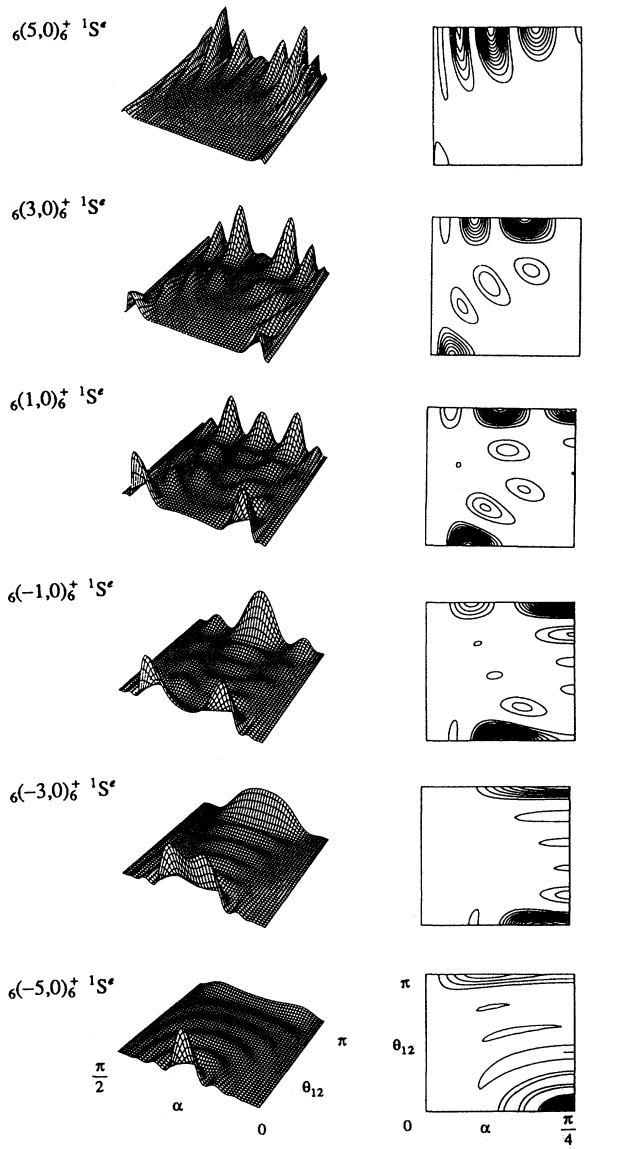

FIG. 4. Similar to Fig. 2 except for all the states within the ${}_6(K,0)_6^+ \ {}^1S^e$ manifold. States with smaller K (larger v) have more nodal lines along the θ_{12} axis.

TABLE IV. Oscillator strengths of ${}_6(K,0)_6^+$ $^1S^e$ states of Ar^{16+} within the $6l6l$ $^1S^e$ manifold. The final states are ${}_6(K,T)_N$ $^1P^o$. For each N, the entries $v_f=v_i$ are underlined. Within the final ${}_6(K,T)_N$ $^1P^o$ manifold for a given N, if the oscillator strength to a given state is less than 2% of the maximum value in that manifold, the entry is left blank.

			$(K,T)=(5,0)$	(3,0)	(1,0)	(−1,0)	(−3,0)	(−5,0)
			$v_i=0$	2	4	6	8	10
N	(K,T)	v_f	10^2f	10^2f	10^2f	10^2f	10^2f	10^2f
1	(0,0)	0	1.57	0.13	0.01	0.06	0.09	0.07
2	(1,0)	0	5.09		0.05	0.04		
	(0,1)	1	1.04	0.43	0.48	0.16		
	(−1,0)	2	0.33	3.14	0.62	0.13	1.02	1.18
3	(2,0)	0	14.77					
	(1,1)	1	1.56	3.20	0.62			
	(0,0)	2		11.64		0.73	0.24	
	(−1.1)	3		2.53	8.13	3.27	0.59	4.09
	(−2,0)	4		0.73	0.50	0.33	2.75	3.51
4	(3,0)	0	42.50	1.25				
	(2,1)	1	2.25	10.40				
	(1,0)	2		40.68	2.56			
	(0,1)	3		5.12	28.60	1.01	0.21	
	(−1,0)	4			23.08	2.38	4.47	
	(−2,1)	5			4.25	2.31	9.46	7.20
	(−3,0)	6			1.77	37.37	0.20	36.19

the ${}_6(5,0)_6^+$ rotor series are shown in Table VI. Each member in this rotor series has $v_i=0$. It is clear that the total radiative yield is about 15% and the total Auger yield is about 85% for both states. This is essentially identical to the branching ratios shown in Table I for the $^1S^e$ state, which is the first member of the rotor series.

The propensity rule $\Delta v=0$ for radiative and Auger decays also holds for these states. In Table VII, the individual dominant $\Delta v=0$ radiative decay channels are shown of the first three excited states along the ${}_6(5,0)_6^+$ rotor series. Each initial state can decay to final states with $\Delta S=0$, $\Delta L=1,0,-1$, and a change in parity. The partial radiative rate decreases rapidly with increasing inner principal quantum numbers N. For $\Delta L=0$ transitions the radiative decay is negligible since the condition $\Delta v=0$ cannot be satisfied. In other words, for $^3P^e$, $^1D^o$ and $^3F^e$ symmetries there are no $v_f=0$ states (the lowest states have $v_f=1$ in each case). Table VII also shows that $L\rightarrow L-1$ transitions are more favorable than $L\rightarrow L+1$ transitions for each N of the final states. This latter fact is well known for the radiative decay of singly excited states.

The same $\Delta v=0$ propensity rule also applies to Auger decays. Figure 5, which is similar to Fig. 3 except for the $(5,0)^+$ $^3P^o$ state, displays that the propensity rule $\Delta v=0$ applies, especially for higher N.

D. Auger widths along the rotor series and along the double-Rydberg series

The systematics of Auger widths along the rotor series were examined previously[6] for low doubly excited states for low-Z atoms and ions. It was found that the Auger width remains nearly constant along the rotor series until near the end of the series. This is further illustrated in Fig. 6 where the widths of the ${}_N(N-1,0)_N^+$ rotor series for $N=6$, 8, and 10 are shown. Along the double-Rydberg series (the vertical sequence in Fig. 6), however, the widths do not decrease smoothly with increasing N as in the usual Rydberg series. In fact, Fig. 6 shows that the width for the $N=10$ rotor series is actually broader than the width for the $N=6$ rotor series. This irregularity can be quite pronounced locally, as displayed in Fig. 7 for the

TABLE V. Partial rates (10^{12} s^{-1}) for the Auger decay to the ${}_\epsilon(K,0)_4$ $^1S^e$ channels from the ${}_6(K,0)_6^+$ $^1S^e$ states of Ar^{16+}. The entries illustrate the propensity rule for autoionization: $v_f=v_i$.

			$(K,T)=$	(5,0)	(3,0)	(1,0)	(−1,0)	(−3,0)	(−5,0)
			$v_i=$	0	2	4	6	8	10
N	(K,T)	v_f							
4	(3,0)	0		21.0	5.7	0.2			
	(1,0)	2		4.7	104.6	10.9	2.0	0.6	
	(−1,0)	4		0.4	8.2	177.3	0.4	2.2	
	(−3,0)	6			7.6	1.4	90.4	32.7	

TABLE VI. Auger rates, radiative rates, and branching ratios of the ${}_6(5,0)_6^+ \ {}^3P^o$ and ${}_6(5,0)_6^+ \ {}^1D^e$ states of Ar^{16+}. Doubly excited states are calculated by CI. (a) Calculated for ${}^3P^o$ and (b) for ${}^1D^e$.

N	Auger energy (Ry)	Auger rate (10^{12} s^{-1})	Branching ratio ($\times 100$)	Radiative rate (10^{12} s^{-1})	Branching ratio ($\times 100$)
			(a) for ${}^3P^o$		
1				3.66	12.9
2	63.40	1.06	3.7	0.87	3.1
3	18.40	4.77	16.9	0.31	1.1
4	2.65	17.37	61.5	0.14	0.5
5				0.07	0.2
Total		23.20	82.1	5.05	17.8
			(b) for ${}^1D^e$		
1				2.97	9.8
2	63.41	1.13	3.7	0.87	2.9
3	18.41	5.29	17.5	0.34	1.1
4	2.66	19.33	64.1	0.16	0.5
5				0.08	0.3
Total		25.75	85.3	4.42	14.6

${}_N(N-1,0)_N^+ \ {}^1S^e$ and ${}_N(N-2,1)_N^+ \ {}^1P^o$ double-Rydberg series. Each state can Auger decay to a number of final $N_f l\epsilon l'$ states. The highest possible N_f, which also accounts for the highest partial Auger width, is also listed in Fig. 7. An anomalously large Auger width occurs whenever the Auger electron energy is quite small. This happens for $(N,N_f)=(3,2)$, $(7,5)$, and $(10,7)$ in Fig. 7. The large width is due to the normalization factor of the continuum Auger electron wave functions. Recall that in Eq. (2) the continuum wave function is normalized per units of energy which has an amplitude proportional to $k_f^{-1/2}$. When k_f is small, the Auger width becomes large. Factoring out this "singularity," a plot of $k_f\Gamma_A$, where $k_f^2/2$ is the Auger energy, would display the desirable smooth dependence of $k_f\Gamma_A$ versus N. This is shown in Fig. 8.

V. SUMMARY AND DISCUSSION

In this article we have studied the radiative and Auger rates of doubly excited states of two-electron ions when both electrons are highly excited. Calculations have been performed for the doubly excited states of Ar^{16+} using the restricted configuration-interaction wave functions. Limiting ourselves to higher Z ions, the configurations included in the CI calculation can be limited to states where the principal quantum numbers n and N are fixed.

Our major goal was to look for propensity rules to identify the dominant final states populated by the radiative and Auger decays. The results indicated that Auger decay dominates for most of the intrashell states studied. However, the highest few states within a given manifold can have comparable radiative and Auger decay rates. Among the possible final states, it was found that the propensity rule $\Delta v = 0$ applies well for both the radiative and the Auger processes, and that the radiative process populates predominantly low-energy states that have large photon energies, while the Auger process populates states that have small Auger energies.

We have examined systematics of the radiative and Auger rates along the vibrational series, the rotor series, and the double-Rydberg series. Along each series, the Auger and radiative rates are expected to vary smoothly. However, for the Auger process local sharp variations

TABLE VII. Dependence of the radiative rates on the total L, S, π, and N of the final states ${}_6(K,T)_N$ for the radiative decay of the ${}_6(5,0)_6^+ \ {}^3P^o$, ${}^1D^e$, and ${}^3F^o$ states of Ar^{16+}.

Final state N	K	T	v_f	Initial state: ${}^3P^o$ ${}^3S^e$	${}^3P^e$	${}^3D^e$	${}^1D^e$ ${}^1P^o$	${}^1D^o$	${}^1F^o$	${}^3F^o$ ${}^3D^e$	${}^3F^e$	${}^3G^e$
1	0	0	0	2.00		1.66	2.24		0.73	1.83		0.05
2	1	0	0	0.47		0.28	0.67		0.12	0.73		0.05
3	2	0	0	0.18		0.12	0.26		0.06	0.28		0.03
4	3	0	0	0.08		0.06	0.12		0.03	0.15		0.02
5	4	0	0	0.04		0.03	0.06		0.02	0.08		0.01
Total				2.77		2.15	3.35		0.96	3.07		0.16

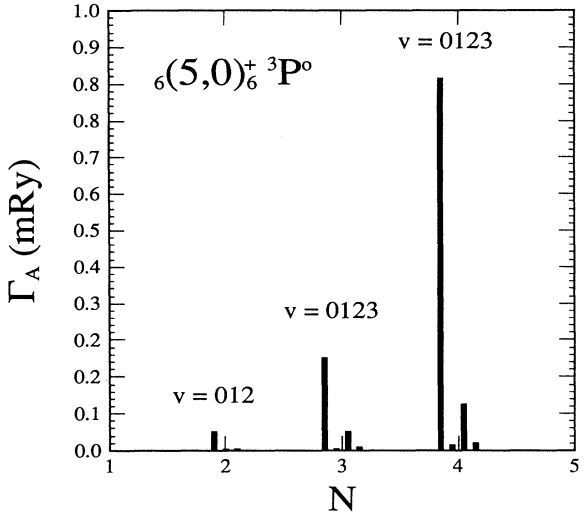

FIG. 5. Similar to Fig. 3 except for the $_6(5,0)_6^+$ $^3P^o$ state.

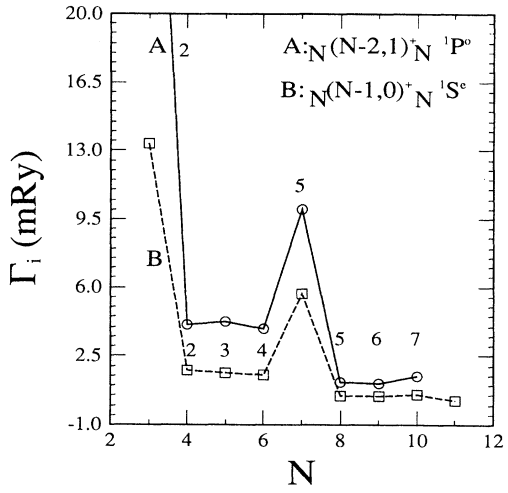

FIG. 7. Total Auger widths along the double-Rydberg series for (A) $_N(N-2,1)_N^+$ $^1P^o$, (B) $_N(N-1,0)_N^+$ $^1S^e$. The highest principal quantum number of the remaining ion after Auger decay is also shown. A sharp increase in the Auger width occurs when the Auger electron energy is very small.

can occur when Auger decay happens to a nearby continuum state with very small kinetic energies. It is not clear whether this sharp structure will disappear after a more completed multichannel calculation. This type of "local" structure makes the interpolation and extrapolation of Auger widths quite difficult along any series as well as its Z dependence. Recent high-resolution photoabsorption spectra of helium atoms obtained using synchrotron radiation shows that the widths of high-lying doubly excited states display modulations due to the intershell coupling in the energy region where such "local" structures are expected. The modulations depend on the excitation mechanism and it is not clear what detailed structures can be expected when these doubly excited states are formed in electron capture processes. Experimental data from such collisions are strongly desirable.

We have limited our study in this article to intrashell states which all have $A=+1$. These states decay primarily by Auger process and radiative decay contributes significantly only for the highest states within a given manifold. It is known from the study of low-Z systems

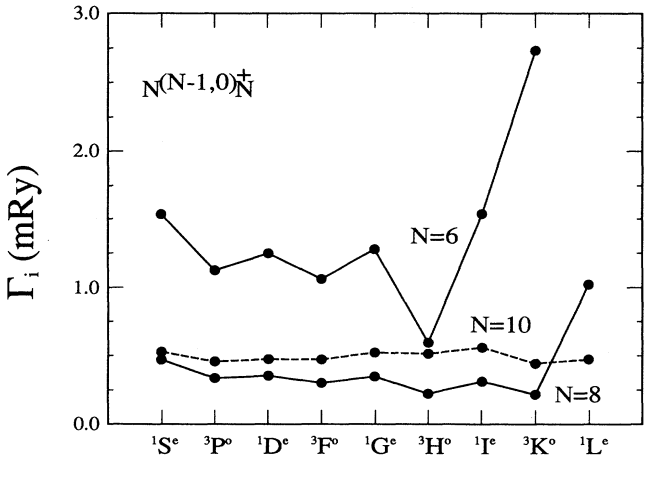

FIG. 6. Total Auger widths along the rotor series for $N=6$, 8, and 10 of the $_N(N-1,0)_N$ double-Rydberg series. Note all the states have $v=0$ and that the width does not decrease smoothly with increasing N.

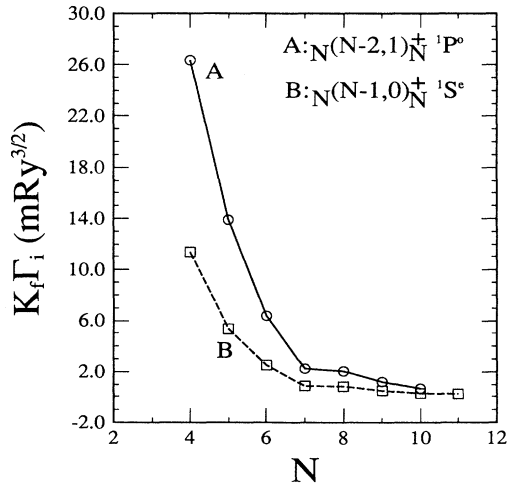

FIG. 8. Rescaling of the Auger widths shown in Fig. 7 by displaying $k_f\Gamma_i$ along the double-Rydberg series. (See text.)

that the Auger widths are much smaller for $A=-1$ and $A=0$ states. For these states the flourescence yield may become non-negligible. Calculations are being carried out for intershell states where this systematics is being examined.

ACKNOWLEDGMENTS

This work is supported in part by the U.S. Department of Energy, Office of Basic Energy Sciences, Division of Chemical Sciences.

---

*Permanent address: Institute of Atomic and Molecular Physics, Jilin University, Changchun, Jilin, People's Republic of China.

[1]N. Morita and T. Suzuki, J. Phys. B **21**, L439 (1988).
[2]P. Camus, T. F. Gallagher, J. M. Lecomte, P. Pillet, and L. Pruvost, Phys. Rev. Lett. **62**, 2365 (1989).
[3]C. D. Lin, Phys. Rev. A **10**, 1986 (1974).
[4]S. Watanabe and C. D. Lin, Phys. Rev. A **34**, 823 (1986).
[5]J. M. Rost and J. S. Briggs, J. Phys. B **23**, L339 (1990).
[6]Z. Chen and C. D. Lin, Phys. Rev. A **40**, 6712 (1989).
[7]M. Matsuzawa, T. Motoyama, H. Fukuda, and N. Koyama, Phys. Rev. A **34**, 1793 (1986).
[8]T. Motoyama, N. Koyama, and M. Matsuzawa, Phys. Rev. A **38**, 670 (1988).
[9]H. Andersson, H. Cederquist, G. Astner, P. Hvelplund, and J. O. P. Pedersen, Phys. Scr. **42**, 150 (1990).
[10]J. P. Briand *et al.*, Phys. Rev. Lett. **65**, 159 (1990).
[11]H. J. Andrä, in *Fundamental Processes of Atomic Dynamics,* edited by J. S. Briggs, H. Kleinpoppen, and H. O. Lutz (Plenum, New York, 1988).
[12]J. E. Hansen, J. Phys. (Paris) Colloq. **50**, C1-603 (1989).
[13]C. D. Lin, Phys. Rev. A **29**, 1019 (1984).
[14]C. D. Lin, Adv. At. Mol. Phys. **22**, 77 (1986).
[15]D. R. Herrick and O. Sinanoglu, Phys. Rev. A **11**, 97 (1975).
[16]C. D.Lin, Phys. Rev. A **25**, 26 (1982).
[17]L. Lipsky, R. Anania, and M. J. Conneely, At. Data Nucl. Data Tables **20**, 127 (1977).
[18]C. A. Nicolaides and Y. Komninos, Phys. Rev. A **35**, 999 (1987).
[19]Z. Chen and C. D. Lin, J. Phys. B **22**, 2875 (1989).
[20]Y. K. Ho, Phys. Rev. A **23**, 2137 (1981).
[21]H. Bachau, J. Phys. B **17**, 1771 (1984).
[22]M. Mack *et al.*, Phys. Rev. A **39**, 3846 (1989).
[23]Z. Chen and C. D. Lin, J. Phys. B **22**, 2875 (1989).
[24]P. G. Harris *et al.*, Phys. Rev. Lett. **65**, 309 (1990).
[25]H. R. Sadeghpour and C. H. Greene, Phys. Rev. Lett. **65**, 313 (1990).
[26]M. Domke, Phys. Rev. Lett. **66**, 1306 (1991).